



Andreev reflection and Josephson effect in the $\alpha - T_3$ latticeXingfei Zhou **New Energy Technology Engineering Laboratory of Jiangsu Province, School of Science,
Nanjing University of Posts and Telecommunications, Nanjing 210023, China* (Received 25 May 2021; revised 19 September 2021; accepted 20 September 2021; published 28 September 2021)

We investigate the Andreev reflection and the Josephson effect in the $\alpha - T_3$ lattice, which falls between graphene ($\alpha = 0$) and the dice lattice ($\alpha = 1$), by adjusting the parameter α . In the regime of the specular Andreev reflection, when the incident energy of the electron is small, the probability of Andreev reflection decreases as the parameter α increases. On the contrary, when the incident energy is large, the probability of Andreev reflection increases as the parameter α increases. Interestingly, when the incident energy approaches the superconducting energy gap function, the Andreev reflection with approximate all-angle perfect transmission happens in the case of $\alpha = 1$. In the regime of Andreev retroreflection, when the parameter α increases, the probability of Andreev reflection increases regardless of the value of incident energy. When the incident energy approaches the superconducting energy gap function, the Andreev reflection with approximate all-angle perfect transmission happens regardless of the value of α . We also give the differential conductance in these two regimes and find that it increases as the parameter α increases generally. In addition, the $\alpha - T_3$ lattice-based Josephson current increases as α increases. When the length of the junction approaches zero, the critical Josephson currents in the different values of α approach the same value.

DOI: [10.1103/PhysRevB.104.125441](https://doi.org/10.1103/PhysRevB.104.125441)**I. INTRODUCTION**

With the rise of graphene [1], the honeycomblike lattices such as silicene, two-dimensional transition metal dichalcogenides, and black phosphorus have been researched widely due to expected nanotechnology applications in the future [2–5]. There is a special honeycomblike lattice named the $\alpha - T_3$ lattice whose geometry is an additional atom sitting at the center of each hexagon [6–11], shown in Fig. 1(a). The continuous evolution of α from 0 to 1 can be linked to a smooth transition from graphene (pseudospin $S = \frac{1}{2}$) to a dice or T_3 lattice (pseudospin $S = 1$). Recently, the material $\text{Hg}_{1-x}\text{Cd}_x\text{Te}$ at the critical doping could be mapped onto the $\alpha - T_3$ lattice with the parameter $\alpha = 1/\sqrt{3}$ [12]. The Hamiltonian of the $\alpha - T_3$ lattice is described by the Dirac-Weyl equation, and its electronic structure consists of a pair consisting of a linear Dirac cone and a flat band passing through the Dirac point exactly.

The variable Berry phase (from π to 0) in the $\alpha - T_3$ lattice has attracted many researchers to investigate Berry-phase-based electronic properties such as Berry-phase-dependent direct current (DC) Hall conductivity [13], Berry-phase-modulated valley-polarized magnetoconductivity [14], and the photoinduced valley and electron-hole symmetry breaking [15]. Someone even designed a chaos-based Berry phase detector in the $\alpha - T_3$ lattice [16]. There are also many unusual electronic properties to be discussed such as the minimal conductivity [17,18], super-Klein tunneling [19–22], magneto-optical conductivity and the Hofstadter butterfly

[23–25], gap generation and flat band catalysis [26,27], nonlinear optical response [28], thermoelectric performance in a nanoribbon made of a $\alpha - T_3$ lattice [29], topological phase transition [30–34], and electronic and optical properties in the irradiated $\alpha - T_3$ lattice [35,36]. In addition, flat-band-induced diverging DC conductivity [37], nontrivial topology [38–43], and ferromagnetism were studied [44,45].

Unfortunately, the Andreev reflection and Josephson effect, as important transport properties in condensed matter physics, are not discussed in the $\alpha - T_3$ lattice. The Andreev reflection was described as the electron-hole conversion at the interface of the normal metal-superconductor [46]. Beenakker [47] discussed the Andreev reflection in a graphene-based superconducting junction and found that the electron-hole conversion in different bands (interband conversion) leads to the specular Andreev reflection (SAR), which is different from the case in a general metal-superconductor junction where only Andreev retroreflection (ARR) happens in the same band (intraband conversion) [46]. After that, many researchers focused on the Andreev reflection in graphenelike materials such as silicene [48], MoS_2 [49], and phosphorene [50]. Recently, the anomalous Andreev reflection, interband (intraband) conversion-induced ARR (SAR) was found in an 8-*Pmmn* borophene-based superconducting junction [51].

Josephson [52,53] predicted that the supercurrent carried by Cooper pairs will tunnel in a sandwich structure which is made of two superconductors (with different macroscopic phases) separated by a thin insulating barrier. His theory was verified in experiment by Anderson and Rowell. [54], and this effect was named the Josephson effect. When the insulating barrier is replaced by a normal metal, based on Andreev reflection, some split energy levels below the energy gap of the

*zxf@njupt.edu.cn

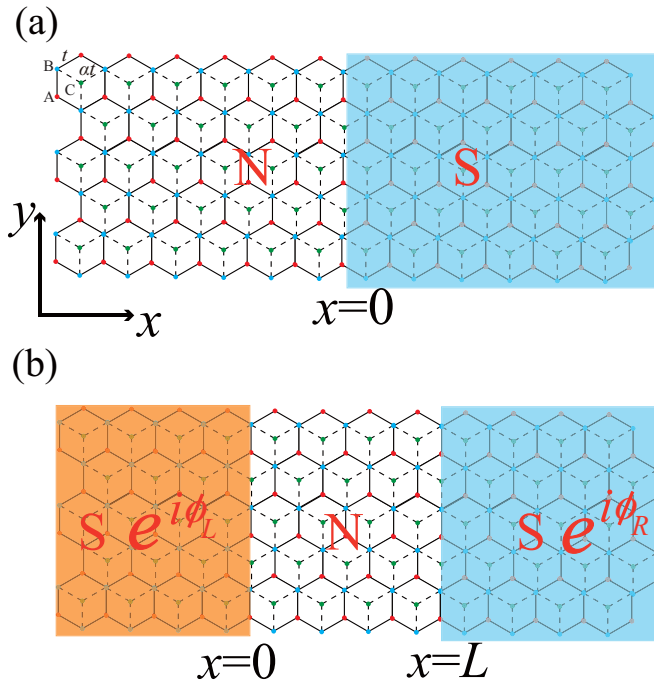


FIG. 1. (a) $\alpha - T_3$ lattice-based normal metal-superconductor (NS) junction and (b) superconductor-normal metal-superconductor (SNS) junction. There are three atoms per unit cell at sites A (red) and B (blue), connected via hopping t , and an additional site C (green) at the center of the hexagons, connected with B via a variable hopping parameter αt . $\phi_{L(R)}$ is the macroscopic phase in the left (right) superconducting region.

superconductor are produced in the normal metal. These split energy levels are called Andreev bound states, which support the transport of Cooper pairs between the left and right superconductors and then generate supercurrent [55]. Generally, by calculating the phase-difference-dependent Josephson free energy, the minimal Josephson free energy appears at phase difference $\phi = 0$, and this Josephson junction is called the 0 junction. If the middle region is a ferromagnetic metal, i.e., superconductor-ferromagnet-superconductor junction, the direction of the critical supercurrent will be reversed, which was predicted by Buzdin *et al.* [56] and later reviewed by Buzdin [57]. In this case, the minimal Josephson free energy appears at phase difference $\phi = \pi$, and this Josephson junction is called the π junction, which is suggested as a promising device to realize qubits [58,59]. The φ junction, the minimal Josephson free energy at the phase difference $\phi = \pm\varphi$, was predicted and observed in a structure consisting of periodic alternating 0 and π junctions [60,61]. The φ_0 junction, the minimal Josephson free energy at the phase difference $\phi = \varphi_0$, was discussed in the nanowire-based Josephson junction applied by the Rashba spin-orbit coupling and the Zeeman field [62,63], the helical edge states of a quantum spin-Hall insulator applied by the magnetic field [64], the magnetized topological insulator interfaces [65], and the silicene nanoribbon applied by an antiferromagnetic exchange magnetization or irradiated by a circularly polarized off-resonant light [66]. These Josephson junctions play an important role in the design

of superconducting circuits, which stimulates researchers to study the Josephson effect constantly.

We find that the Andreev reflection was investigated in the case of $\alpha = 0$ (such as graphene [47]) and $\alpha = 1$ (such as the T_3 lattice [67]), while the Josephson effect was only studied in the case of $\alpha = 0$ (such as graphene [68]). Therefore, an interesting question to discuss the continuous evolution of the Andreev reflection and the Josephson effect from $\alpha = 0$ to 1 is lacking, which inspires us to discuss the Andreev reflection and the Josephson effect in the $\alpha - T_3$ lattice. We firstly give the model and basic formalism. Then the numerical results and theoretical analysis about the probability of Andreev reflection, the differential conductance, and the Josephson effect are presented and discussed. Finally, the main results of this paper are summarized.

II. MODEL AND FORMALISM

The Bogoliubov-de Gennes (BdG) equation in the $\alpha - T_3$ lattice-based superconducting junction shown in Fig. 1(a) is written as [47,69]

$$\begin{pmatrix} \mathcal{H} - E_F & \Delta_0 e^{i\phi} \sigma_0 \\ \Delta_0 e^{-i\phi} \sigma_0 & E_F - \mathcal{T}HT^{-1} \end{pmatrix} \begin{pmatrix} u_e \\ v_h \end{pmatrix} = \varepsilon \begin{pmatrix} u_e \\ v_h \end{pmatrix}. \quad (1)$$

Here, E_F is the Fermi energy of system; ϕ is the macroscopic phase in the superconducting region; $\mathcal{T} = \sigma_x \otimes \tau \mathcal{C}$ is the time-reversal operator, with σ_x the Pauli matrix, $\tau = \begin{pmatrix} 1 & 0 & 0 \\ 0 & -1 & 0 \\ 0 & 0 & 1 \end{pmatrix}$, and \mathcal{C} the operator of complex conjugation; ε is the excited energy of electron and hole; u_e and v_h are the electron (electronlike) and hole (holelike) wave functions in the normal (superconducting) region, respectively; Δ_0 is the zero temperature energy gap function, which is induced in the $\alpha - T_3$ lattice by approaching a conventional s-wave superconductor; and σ_0 denotes a unit matrix. The Hamiltonian in the $\alpha - T_3$ lattice is

$$\mathcal{H} = \begin{pmatrix} \mathcal{H}_+ & 0 \\ 0 & \mathcal{H}_- \end{pmatrix}, \quad (2)$$

in which $\mathcal{H}_\pm = \hbar v_F \mathbf{S} \cdot \mathbf{k} + U(x)$ with

$$S_x = \pm \begin{pmatrix} 0 & \cos \varphi & 0 \\ \cos \varphi & 0 & \sin \varphi \\ 0 & \sin \varphi & 0 \end{pmatrix}, \quad \text{and} \quad (3)$$

$$S_y = -i \begin{pmatrix} 0 & \cos \varphi & 0 \\ -\cos \varphi & 0 & \sin \varphi \\ 0 & -\sin \varphi & 0 \end{pmatrix}. \quad (4)$$

Here, the Fermi velocity $v_F = 10^6$ m/s, the label \pm denotes the K and K' valleys, respectively, the angle φ is related to the strength of the coupling α as $\alpha = \tan \varphi$, and $U(x) = -U_0 \Theta(x)$ with the Heaviside step function Θ can be adjusted by doping or a gate voltage in the superconducting region and is zero in the normal region.

Owing to the time-reversal symmetry of the $\alpha - T_3$ lattice, the Hamiltonian is time-reversal invariant, i.e., $\mathcal{T}HT^{-1} = \mathcal{H}$. Then by matrix transformation, Eq. (1) can be decoupled into

two sets of six equations with the form

$$\begin{pmatrix} \mathcal{H}_\pm - E_F & \Delta_0 e^{i\phi} \sigma_0 \\ \Delta_0 e^{-i\phi} \sigma_0 & E_F - \mathcal{H}_\pm \end{pmatrix} \begin{pmatrix} u_e \\ v_h \end{pmatrix} = \varepsilon \begin{pmatrix} u_e \\ v_h \end{pmatrix}. \quad (5)$$

For the convenience of discussion, we consider the set with \mathcal{H}_+ because of the valley degeneracy. The uniform spectrum is written as $\varepsilon = \sqrt{(E_F + U(x) \pm \hbar v_F |k|)^2 + \Delta_0^2 \Theta(x)}$, with $|k| = \sqrt{k_x^2 + k_y^2}$ in both normal and superconducting regions. When ε and transverse momentum k_y are given, we obtain four eigenstates in the normal region by solving Eq. (5):

$$\begin{aligned} \psi_e^\pm &= \exp(\pm i k_{xe} x + i k_y y) \\ &\quad \times (\pm e^{\mp i\theta} \cos \varphi, 1, \pm e^{\pm i\theta} \sin \varphi, 0, 0, 0)^T, \\ \psi_h^\pm &= \exp(\pm i k_{xh} x + i k_y y) \\ &\quad \times (0, 0, 0, \mp e^{\mp i\theta'} \cos \varphi, 1, \mp e^{\pm i\theta'} \sin \varphi)^T. \end{aligned} \quad (6)$$

The state ψ_e^+ (ψ_h^+) denotes the electron (hole) moves in the $+x$ direction [toward the normal metal-superconductor (NS) junction], while ψ_e^- (ψ_h^-) denotes the electron (hole) moves in the $-x$ direction (away from the NS junction). The angles $\theta = \arcsin[\hbar v_F k_y / (\varepsilon + E_F)]$ and $\theta' = \arcsin[\hbar v_F k_y / (\varepsilon - E_F)]$ are the incident angle of an electron and the reflected angle of the corresponding hole, respectively. The wave vector k_{xe} (k_{xh}) is the longitudinal wave vector of the electron (hole). We consider the regime of $U_0 \gg E_F$ and ε in the superconducting region; then the simplified wave functions are obtained as

$$\psi_S^\pm = \begin{pmatrix} e^{\pm i\beta} \\ \pm \frac{1}{\cos \varphi} e^{\pm i\beta} \\ \tan \varphi e^{\pm i\beta} \\ e^{-i\phi} \\ \pm \frac{1}{\cos \varphi} e^{-i\phi} \\ \tan \varphi e^{-i\phi} \end{pmatrix} \exp(\pm i k_0 x + i k_y y - \kappa x). \quad (7)$$

Here, $k_0 = U_0 / \hbar v_F$, $\kappa = (\Delta_0 / \hbar v_F) / \sin \beta$, and β is defined as

$$\beta = \begin{cases} \arccos\left(\frac{\varepsilon}{\Delta_0}\right) & \varepsilon < \Delta_0, \\ -i \operatorname{arccosh}\left(\frac{\varepsilon}{\Delta_0}\right) & \varepsilon > \Delta_0. \end{cases} \quad (8)$$

The state ψ_S^+ (ψ_S^-) represents the wave function of a quasihole (quasielectron) for $\varepsilon > \Delta_0$, while this state is the coherent superposition of the electron and hole excitations for $\varepsilon < \Delta_0$ in the superconducting region. According to the derivation of probability current in Ref. [51], assuming a wave function in the general form $\Psi = (\psi_A, \psi_B, \psi_C)^T$, the x component of the probability current is $J_x = 2\operatorname{Re}[\psi_B^* (\psi_A \cos \varphi + \psi_C \sin \varphi)]$. By using the method in Refs. [7,20,21], the wave function ψ_B and the linear combination $\psi_A \cos \varphi + \psi_C \sin \varphi$ are continuous across an interface, which corresponds to the conservation of the probability current J_x . Therefore, the matching conditions for the wave functions across the $\alpha - T_3$ lattice-based interface ($x = 0$) are

$$\begin{aligned} \psi_B|_{x=0^+} &= \psi_B|_{x=0^-}, \\ \psi_A \cos \varphi|_{x=0^+} + \psi_C \sin \varphi|_{x=0^+} &= \psi_A \cos \varphi|_{x=0^-} + \psi_C \sin \varphi|_{x=0^-}. \end{aligned} \quad (9)$$

The wave functions in the normal and superconducting regions are given as

$$\begin{aligned} \Psi_N &= \psi_e^+ + r \psi_e^- + r_A \psi_h^-, \\ \Psi_S &= a \psi_S^+ + b \psi_S^-, \end{aligned} \quad (10)$$

where r is the reflected amplitude for an incident electron, r_A is the reflected amplitude for a reflected hole, and a (b) is the transmitted amplitude for an electronlike (holelike) quasiparticle. Using the matching conditions in Eq. (9) at $x = 0$, a system of four equations is obtained:

$$\begin{aligned} 1 + r &= \frac{1}{\cos \varphi} (a e^{i\beta} - b e^{-i\beta}), \\ \chi_{ei} + r \chi_{er} &= \frac{1}{\cos \varphi} (a e^{i\beta} + b e^{-i\beta}), \\ r_A &= \frac{1}{\cos \varphi} (a e^{-i\phi} - b e^{-i\phi}), \\ r_A \chi_{hr} &= \frac{1}{\cos \varphi} (a e^{-i\phi} + b e^{-i\phi}). \end{aligned} \quad (11)$$

Here, $\chi_{ei(er)}$ and χ_{hr} in the above equations are given

$$\begin{aligned} \chi_{ei} &= e^{-i\theta} \cos^2 \varphi + e^{i\theta} \sin^2 \varphi, \\ \chi_{er} &= -e^{i\theta} \cos^2 \varphi - e^{-i\theta} \sin^2 \varphi, \\ \chi_{hr} &= e^{i\theta'} \cos^2 \varphi + e^{-i\theta'} \sin^2 \varphi. \end{aligned} \quad (12)$$

By solving Eq. (11), we have the amplitudes of the normal and Andreev reflections, respectively:

$$\begin{aligned} r &= \frac{(\chi_{ei} - \chi_{hr}) \cos \beta + i(\chi_{ei} \chi_{hr} - 1) \sin \beta}{(\chi_{er} - \chi_{hr}) \cos \beta + i(\chi_{er} \chi_{hr} - 1) \sin \beta}, \\ r_A &= \frac{\chi_{er} - \chi_{ei}}{(\chi_{ei} - \chi_{hr}) \cos \beta + i(\chi_{er} \chi_{hr} - 1) \sin \beta}. \end{aligned} \quad (13)$$

In this paper, the probability current is conserved in the x direction. Then by using the same derivation in Ref. [51], the corresponding incident probability current of the electron along the x direction is $J_{xei} = \chi_{ei} + \chi_{ei}^*$, the corresponding reflected probability current of the electron is $J_{xer} = \chi_{er} + \chi_{er}^*$, and the corresponding reflected probability current of hole is $J_{xhr} = \chi_{hr} + \chi_{hr}^*$. Thus, the reflected and Andreev reflected probabilities are written as $R = |J_{xer} / J_{xei}| r^*$ and $R_a = |J_{xhr} / J_{xei}| r_a^*$, respectively.

III. RESULTS AND ANALYSIS

A. Andreev reflected probability

In Fig. 2, the incident angle of the electron-dependent Andreev reflected probability is plotted with the different incident energies and the different values of α in $E_F = 0$. In Fig. 2(a), the Andreev reflected probability decreases as α increases when the incident energy is equal to $0.2\Delta_0$. With the increase of the incident energy, shown in Figs. 2(b)–2(d), the Andreev reflected probability has a trend that its value increases as α increases. We choose a limit value of the incident energy ($\varepsilon = 0.99\Delta_0$) in Fig. 3. Then this phenomenon, i.e., R_a increases as α increases, is obvious. Interestingly, an approximately perfect transmission ($R_a = 1$) in a wide range

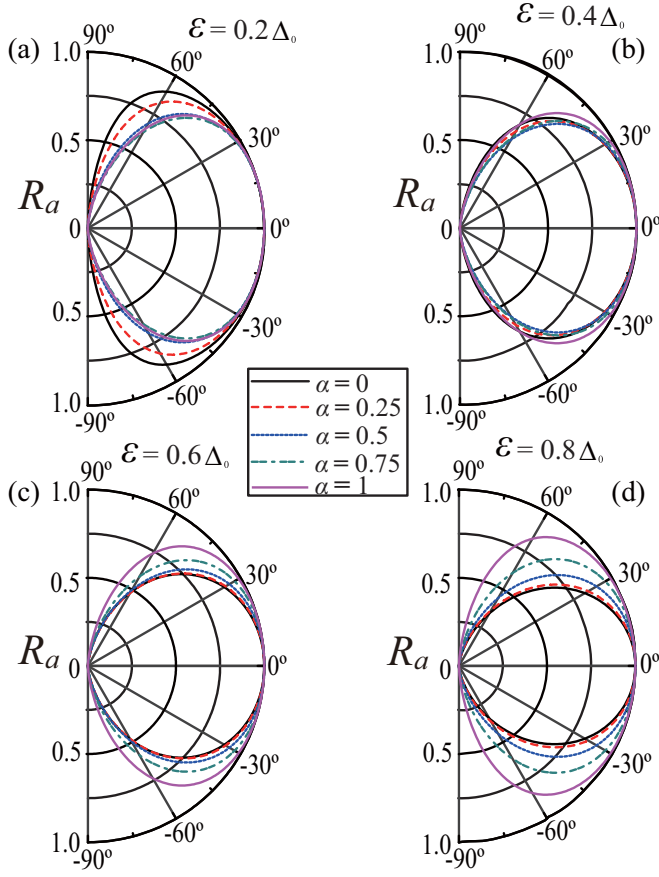


FIG. 2. (a)–(d) The incident angle of electron-dependent Andreev reflected probability in the case of different incident energies and different values of α . Here, $\Delta_0 = 1$ meV, $U_0 = 150\Delta_0$, and $E_F = 0$.

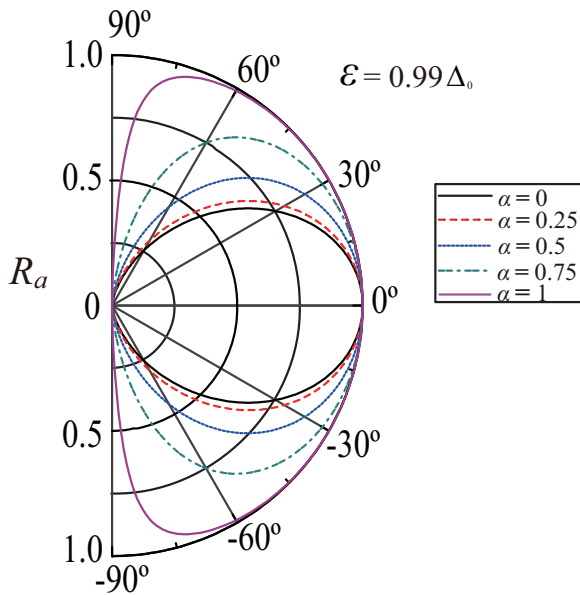


FIG. 3. The incident angle of the electron-dependent Andreev reflected probability in the case of different values of α with the incident energy $\epsilon = 0.99\Delta_0$. The other parameters are the same as the ones in Fig. 2.

of incident angles is shown when $\alpha = 1$ in Fig. 3, which is called a super-Andreev reflection by some researchers [67].

Let us do some qualitative analysis. In the case of $E_F = 0$, it is easy to obtain $\theta' = \theta$. Then from Eq. (13), we give the Andreev reflected probability:

$$R_a = \frac{4 \cos^2 \theta}{X \cos^2 \beta + Y \sin^2 \beta + Z}, \quad (14)$$

in which X , Y , and Z are defined as

$$\begin{aligned} X &= 4(1 - \sin^2 \theta \sin^2 2\varphi), \\ Y &= 4 \cos^2 \theta + \sin^4 \theta \sin^4 2\varphi, \\ Z &= \sin 4\varphi \sin 2\beta \sin^3 \theta \sin 2\varphi. \end{aligned} \quad (15)$$

In the case of $\epsilon \ll \Delta_0$, we obtain $\cos \beta \rightarrow 0$, while $\sin \beta \rightarrow 1$ by a simple calculation. The Andreev reflected probability becomes

$$R_a \rightarrow \frac{4 \cos^2 \theta}{4 \cos^2 \theta + \sin^4 \theta \sin^4 2\varphi}. \quad (16)$$

Obviously, the Andreev reflected probability decreases as α increases. When α approaches 0, then $\sin^4 2\varphi \rightarrow 0$ in Eq. (16), and then $R_a \rightarrow 1$. These results are consistent with the ones in Fig. 2(a). When the incident energy ϵ approaches Δ_0 , then $\cos \beta \rightarrow 1$, while $\sin \beta \rightarrow 0$. The Andreev reflected probability becomes

$$R_a \rightarrow \frac{\cos^2 \theta}{1 - \sin^2 \theta \sin^2 2\varphi}. \quad (17)$$

We can easily obtain a conclusion that the Andreev reflected probability increases as α increases, and $R_a \rightarrow 1$ when α approaches 1, which are consistent with the results in Figs. 2(d) and 3. We will show that this property does not only happen in $\alpha = 1$ in the next paragraph. In fact, this property can happen regardless of the value of α in the proper parameters.

In Fig. 4, the incident angle of the electron-dependent Andreev reflected probability is plotted with the different incident energies and the different values of α in $E_F = 100\Delta_0$. The Andreev reflected probability increases as α decreases regardless of the value of the incident energy. However, when $\epsilon = 0.99\Delta_0$ in Fig. 5, the super-Andreev reflection is shown regardless of the value of α . The range of incident angles of the super-Andreev reflection increases as α increases. Similarly, some qualitative analyses are given below. When $E_F \gg \epsilon$, we can get $\theta' \approx -\theta$, and then the Andreev reflected probability is written as

$$R_a \rightarrow \frac{4 \cos^2 \theta}{4 \cos^2 \theta + [(2 - \sin^2 \theta \sin^2 2\varphi)^2 - 4 \cos^2 \theta] \sin^2 \beta}. \quad (18)$$

In this equation, the value of $\sin^2 2\varphi$ increases as α increases, which leads to the fact that R_a increases as α increases. This conclusion corresponds with the numerical result in Fig. 4. For clarity, we consider $\epsilon \ll \Delta_0$. Then $\sin \beta \rightarrow 1$, and the Andreev reflected probability becomes

$$R_a \rightarrow \frac{4 \cos^2 \theta}{(2 - \sin^2 \theta \sin^2 2\varphi)^2}. \quad (19)$$

Thus, it is easy to find that R_a increases as α increases, which is consistent with the result in Fig. 4(a). When ϵ approaches

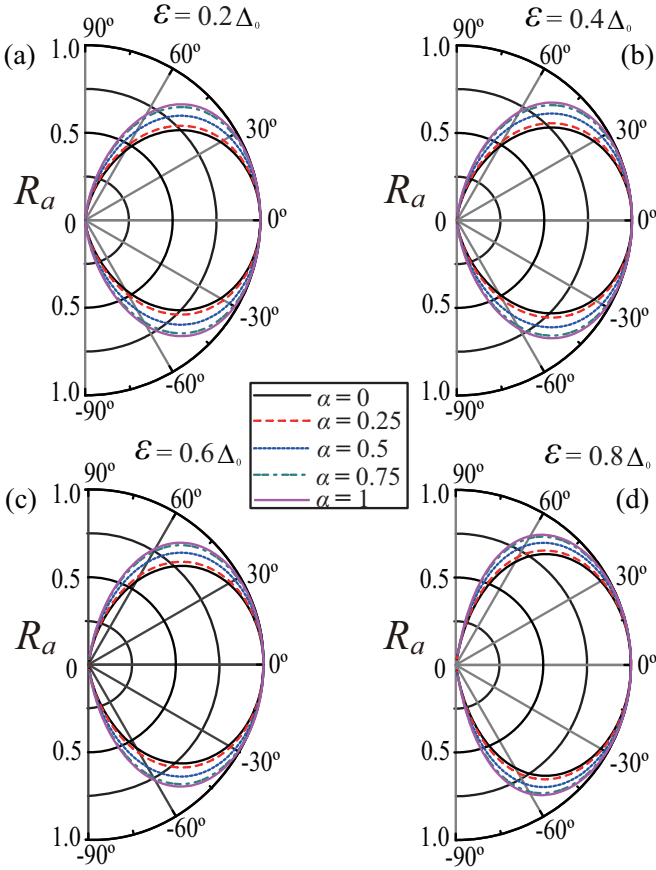


FIG. 4. (a)–(d) The incident angle of the electron-dependent Andreev reflected probability in the case of different incident energies and different values of α . Here, $E_F = 100\Delta_0$, $U_0 = 150\Delta_0$, and the other parameters are the same as the ones in Fig. 2.

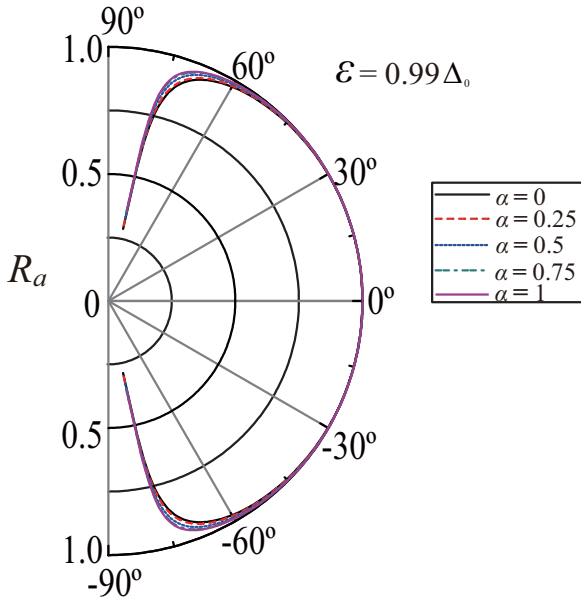


FIG. 5. The incident angle of the electron-dependent Andreev reflected probability in the case of the different values of α with the incident energy $\varepsilon = 0.99\Delta_0$ and $U_0 = 150\Delta_0$. The other parameters are the same as the ones in Fig. 4.

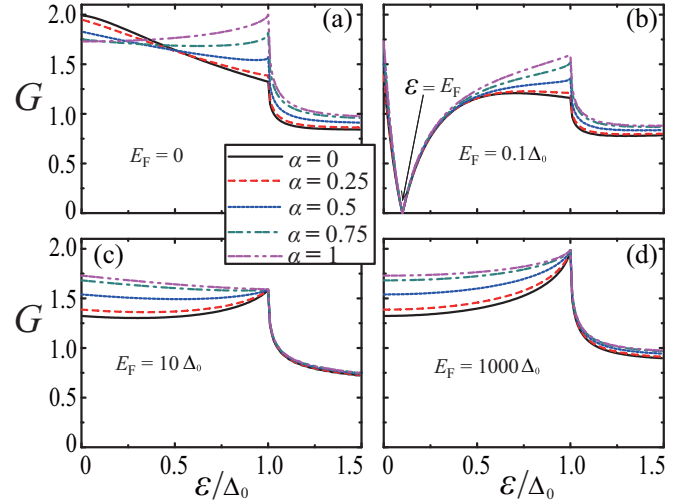


FIG. 6. (a)–(d) The incident energy-dependent differential conductance of the normal metal-superconductor (NS) junction in the case of different Fermi energies. The unit for differential conductance is G_0 . The other parameters are the same as the ones in Fig. 2.

Δ_0 , then $\sin \beta \rightarrow 0$, and the Andreev reflected probability [Eq. (18)] becomes $R_a \rightarrow 1$ regardless of the value of α , which is consistent with the result in Fig. 5. In Ref. [67], the authors give a conclusion that the super-Andreev reflection cannot appear in $\alpha = 0$. Thus, in this paper, we deepen their research.

B. Differential conductance of the NS junction

In the regime of zero temperature, the differential conductance of the NS junction following the Blonder-Tinkham-Klapwijk formula is [70]

$$G = G_0 \int_0^{\frac{\pi}{2}} (1 - R + R_a) \cos \theta d\theta. \quad (20)$$

Considering the twofold spin and valley degeneracies, $G_0 = \frac{4e^2}{h} N(\varepsilon)$ is the ballistic conductance with $N(\varepsilon) = \frac{W(\varepsilon + E_F)}{\pi \hbar v_F}$ the transverse modes in the $\alpha - T_3$ lattice with the width W .

The incident energy-dependent differential conductances of the NS junction in the case of different Fermi energies are shown in Fig. 6. In the case of $E_F = 0$, using the relation $R + R_a = 1$ and Eq. (16), we obtain $G \rightarrow 2G_0$ for $\alpha = 0$, $G \rightarrow 1.96G_0$ for $\alpha = 0.25$, $G \rightarrow 1.84G_0$ for $\alpha = 0.5$, $G \rightarrow 1.76G_0$ for $\alpha = 0.75$, and $G \rightarrow [3\sqrt{2} \operatorname{arctanh}(\frac{\sqrt{2}}{2}) - 2]G_0 \approx 1.74G_0$ for $\alpha = 1$ when $\varepsilon \ll \Delta_0$. When the incident energy ε approaches Δ_0 , using Eq. (17), we get $G \rightarrow \frac{4}{3}G_0$ for $\alpha = 0$, which reproduces the result in the graphene-based superconducting junction, and the formula below for $\alpha \neq 0$:

$$G \rightarrow \frac{2[\sin 2\varphi - \cos^2 2\varphi \operatorname{arctanh}(\sin 2\varphi)]}{\sin^3 2\varphi} G_0. \quad (21)$$

From the formula above, it is easy to obtain that $G \rightarrow 1.4G_0$ for $\alpha = 0.25$, $G \rightarrow 1.58G_0$ for $\alpha = 0.5$, $G \rightarrow 1.83G_0$ for $\alpha = 0.75$, and $G \rightarrow 2G_0$ for $\alpha = 1$. These results are shown in Fig. 6(a).

With the increase of E_F , shown in Figs. 6(b)–6(d), the value of G increases as α increases generally. For $E_F < \Delta_0$, the

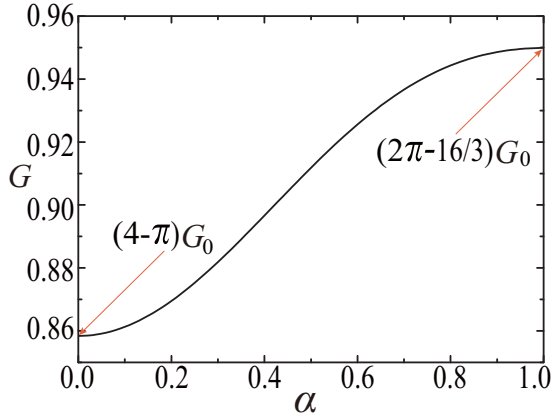


FIG. 7. Parameter α -dependent differential conductance G in the case of $\varepsilon \gg \Delta_0$. The unit for differential conductance is G_0 .

differential conductance vanishes at $\varepsilon = E_F$ regardless of α due to the disappearance of the Andreev reflection, shown in Fig. 6(b). Interestingly, the value of G will tend to $2G_0$ when $\varepsilon \rightarrow \Delta_0$, shown in Fig. 6(d). Now we give a brief analysis below. In the case of $E_F \gg \varepsilon$, when $\varepsilon \ll \Delta_0$, using Eq. (19), $G \rightarrow 4/3G_0 \approx 1.33G_0$ for $\alpha = 0$, which also reproduces the result in the graphene-based superconducting junction, and the formula below for $\alpha \neq 0$:

$$G \rightarrow \frac{\sqrt{2}(2 + \sin^2 2\varphi) \operatorname{arctanh}\left(\frac{\sin 2\varphi}{\sqrt{2}}\right) - 2 \sin 2\varphi}{\sin^3 2\varphi} G_0. \quad (22)$$

By a simple calculation, $G \rightarrow 1.4G_0$ for $\alpha = 0.25$, $G \rightarrow 1.55G_0$ for $\alpha = 0.5$, $G \rightarrow 1.69G_0$ for $\alpha = 0.75$, and $G \rightarrow [3\sqrt{2} \operatorname{arctanh}(\frac{\sqrt{2}}{2}) - 2]G_0 \approx 1.74G_0$ for $\alpha = 1$. When ε approaches Δ_0 , then $\sin \beta \rightarrow 0$, the Andreev reflected probability becomes $R_a \rightarrow 1$, and the reflected probability becomes $R \rightarrow 0$ regardless of the value of α . Thus, the value of G tends to $2G_0$ regardless of the value of α . These results can be verified in Fig. 6(d).

When $\varepsilon \gg \Delta_0$, then $R_a \rightarrow 0$, $\sin \beta \rightarrow -i\frac{\varepsilon}{\Delta_0}$, $\cos \beta \rightarrow \frac{\varepsilon}{\Delta_0}$, and the reflected probability is written as

$$R \rightarrow \frac{(\cos \theta - 1)^2 + (\sin \theta \cos 2\varphi)^2}{(\cos \theta + 1)^2 + (\sin \theta \cos 2\varphi)^2}. \quad (23)$$

We obtain $G \rightarrow (4 - \pi)G_0 \approx 0.86G_0$ for $\alpha = 0$ and $G \rightarrow (2\pi - 16/3)G_0 \approx 0.95G_0$ for $\alpha = 1$, which reproduce the results in Refs. [47,67]. For $\alpha \neq 0$ and 1, the differential conductance G becomes

$$G \rightarrow 2 \csc^2 4\varphi (M - N)G_0, \quad (24)$$

in which M and N are defined as

$$\begin{aligned} M &= 4(\sin^2 2\varphi + \pi \cos^2 2\varphi), \\ N &= \arctan(\cos 2\varphi)(3 + \cos 4\varphi)^2 \sec 2\varphi. \end{aligned} \quad (25)$$

Then we give the α -dependent differential conductance G in Fig. 7. The value of G increases as α increases regardless of the value of E_F [between $(4 - \pi)G_0$ and $(2\pi - \frac{16}{3})G_0$].

C. Josephson current of the superconductor-normal metal-superconductor junction

The $\alpha - T_3$ lattice-based Josephson junction, shown in Fig. 1(b), is also described by Eq. (5) with U_0 applied only in two superconducting regions. The eigenstates in left and right superconducting regions are

$$\begin{aligned} \psi_{\text{SL}}^{\pm} &= \begin{pmatrix} e^{\pm i\beta} \\ \mp \frac{1}{\cos \varphi} e^{\pm i\beta} \\ \tan \varphi e^{\pm i\beta} \\ e^{-i\phi_L} \\ \mp \frac{1}{\cos \varphi} e^{-i\phi_L} \\ \tan \varphi e^{-i\phi_L} \end{pmatrix} \exp(\pm ik_0x + ik_y y + \kappa x), \\ \psi_{\text{SR}}^{\pm} &= \begin{pmatrix} e^{\pm i\beta} \\ \pm \frac{1}{\cos \varphi} e^{\pm i\beta} \\ \tan \varphi e^{\pm i\beta} \\ e^{-i\phi_R} \\ \pm \frac{1}{\cos \varphi} e^{-i\phi_R} \\ \tan \varphi e^{-i\phi_R} \end{pmatrix} \exp(\pm ik_0x + ik_y y - \kappa x). \end{aligned} \quad (26)$$

We analyze the Josephson effect in the experimentally most relevant short-junction regime that the length L of the normal region is smaller than the superconducting coherence length, i.e., $\hbar v_F/L \gg \Delta_0$. The wave functions in the middle and both superconducting regions are given as

$$\begin{aligned} \Psi_{\text{M}} &= f\psi_e^+ + g\psi_e^- + h\psi_h^+ + m\psi_h^-, \\ \Psi_{\text{SL}} &= a\psi_{\text{SL}}^- + b\psi_{\text{SL}}^+, \\ \Psi_{\text{SR}} &= c\psi_{\text{SR}}^- + d\psi_{\text{SR}}^+. \end{aligned} \quad (27)$$

Using the matching conditions in Eq. (9) at $x = 0$ and $x = L$, a system of eight equations is obtained:

$$\begin{aligned} f + g &= \frac{1}{\cos \varphi} (ae^{-i\beta} - be^{i\beta}), \\ f\chi_{ei} + g\chi_{er} &= \frac{1}{\cos \varphi} (ae^{-i\beta} + be^{i\beta}), \\ h + m &= \frac{1}{\cos \varphi} (ae^{-i\phi_L} - be^{-i\phi_L}), \\ h\chi_{hi} + m\chi_{hr} &= \frac{1}{\cos \varphi} (ae^{-i\phi_L} + be^{-i\phi_L}), \\ f' + g' &= \frac{1}{\cos \varphi} (-c'e^{-i\beta} + d'e^{i\beta}), \\ f'\chi_{ei} + g'\chi_{er} &= \frac{1}{\cos \varphi} (c'e^{-i\beta} + d'e^{i\beta}), \\ h' + m' &= \frac{1}{\cos \varphi} (-c'e^{-i\phi_R} + d'e^{-i\phi_R}), \\ h'\chi_{hi} + m'\chi_{hr} &= \frac{1}{\cos \varphi} (c'e^{-i\phi_R} + d'e^{-i\phi_R}), \end{aligned} \quad (28)$$

where $c' = c \exp(-ik_0L - \kappa L)$, $d' = d \exp(ik_0L - \kappa L)$, $f' = f \exp(ik_{xe}L)$, $g' = g \exp(-ik_{xe}L)$, $h' = h \exp(ik_{xh}L)$, $m' = m \exp(-ik_{xh}L)$, and $\chi_{hi} = -e^{-i\theta'} \cos^2 \varphi - e^{i\theta'} \sin^2 \varphi$. To ensure the nonzero solution of Eq. (28), considering $E_F \gg \varepsilon$,

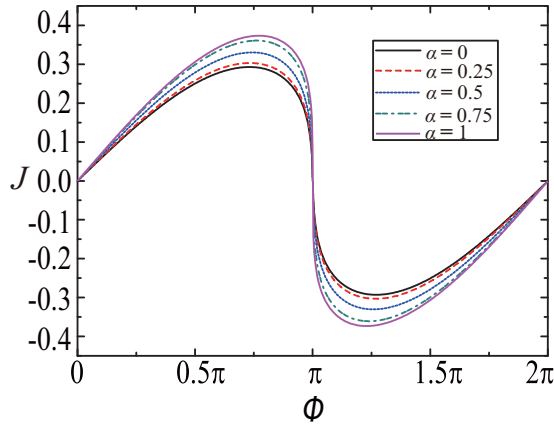


FIG. 8. Phase difference ϕ -dependent Josephson current in the case of the different values of α . Here, $L = 20$ nm, $U_0 = 150\Delta_0$, and $E_F = 100\Delta_0$. The unit for differential conductance is J_0 .

the below condition needs to be satisfied:

$$A \frac{\varepsilon^2}{\Delta_0^2} + B = 0. \quad (29)$$

Parameters A and B are defined as

$$\begin{aligned} A &= (64 \cos^2 \theta - P) \sin^2(k_x L) - 64 \cos^2 \theta, \\ B &= (P - 64 \cos^2 \theta) \sin^2(k_x L) \\ &\quad + 32 \cos^2 \theta (1 + \cos \phi), \end{aligned} \quad (30)$$

where $P = (4 \sin^2 \theta \sin^2 2\phi - 8)^2$, $k_x = \frac{E_F}{\hbar v_F} \cos \theta$, and phase difference $\phi = \phi_R - \phi_L$. We can obtain the Andreev bound level ε from Eq. (29) and then the relation between the Josephson current J passing through the junction with transverse width W and the positive Andreev bound level at zero temperature is given as

$$J = -\frac{4e}{\hbar} \frac{W E_F}{\pi \hbar v_F} \int \frac{d\varepsilon}{d\phi} \cos \theta d\theta, \quad (31)$$

in which the factor of 4 denotes the twofold spin and valley degeneracies. The unit for the Josephson current is $J_0 = \frac{4e}{\hbar} \frac{W E_F}{\pi \hbar v_F} \Delta_0$.

In Fig. 8, the phase difference ϕ -dependent Josephson current is plotted by varying parameter α . The value of the Josephson current increases as α increases. We can give $\frac{d\varepsilon}{d\phi} = -\frac{16 \cos^2 \theta \sin \phi}{\sqrt{-AB}} \Delta_0$ because of $A < 0$. When α increases, the values of $-A$ and B decrease from Eq. (30), then the value of $\frac{d\varepsilon}{d\phi}$ increases, and the increase of the Josephson current is shown in Fig. 8. We also give the length of the junction L -dependent critical Josephson current J_c (the maximal Josephson current) in Fig. 9. The value of J_c oscillates as L varies and increases as α increases. By considering the limiting behavior $L \rightarrow 0$, then $\sin(k_x L) \rightarrow 0$, and the critical Josephson current $J_c \rightarrow \frac{1}{2} J_0$ regardless of the value of α , which is shown in Fig. 9.

IV. DISCUSSIONS AND CONCLUSIONS

In this paper, we have investigated the continuous evolution of the Andreev reflection and the Josephson effect by adjusting the parameter α in the $\alpha - T_3$ lattice system. Now

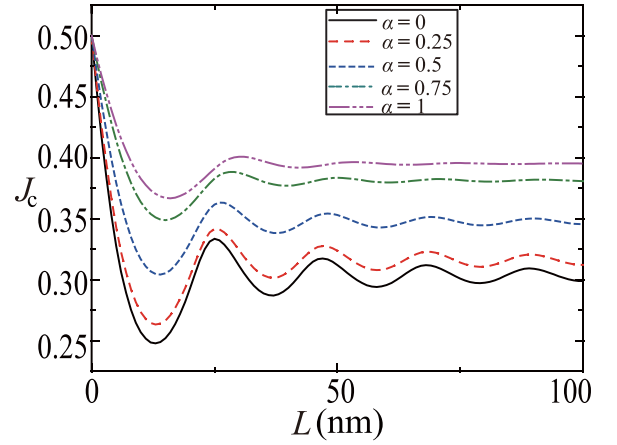


FIG. 9. Length of junction L -dependent critical Josephson current J_c in the case of the different values of α . Here, $E_F = 100\Delta_0$, $U_0 = 150\Delta_0$, and the unit for critical Josephson J_c is J_0 .

we give some discussions about the possible material candidates in experiment. The material $\text{Hg}_{1-x}\text{Cd}_x\text{Te}$ at the critical doping can be mapped onto the $\alpha - T_3$ lattice with parameter $\alpha = 1/\sqrt{3}$ [12]. Additionally, there are several realistic material candidates, including monolayer Mg_2C [71], monolayer Na_2O and K_2O [72], and a trilayer structure of cubic lattices such as $\text{SrTiO}_3/\text{SrIrO}_3/\text{SrTiO}_3$ in the (111) direction [73]. To fabricate a superconducting interface, a conventional s-wave superconductor approaches the $\alpha - T_3$ lattice, and then the superconductivity is induced in the $\alpha - T_3$ lattice by proximity effect.

Finally, we want to mention two open topics. First, for the graphene system, the different pairing symmetry, such as d-wave, f-wave, or p-wave pairings, showed a strong effect on the Andreev reflection and the Josephson effect [74–76]. For the $\alpha - T_3$ lattice, this is an open topic by considering different pairing symmetry in the superconducting region, which could be discussed in future works. Second, the role of the flat band in the Andreev reflection and the Josephson effect is worth discussing. The self-consistent treatment of the pairing amplitude may give us some inspiration [77]. The Fermi energy-dependent superconducting energy gap function was predicted due to the presence of a flat band, which will affect the value of differential conductance and the Josephson current in our work. However, the perfect Andreev reflection (unit efficiency at normal incidence) and the large Andreev reflection effect will not be affected in our work if the incident energy approaches the superconducting energy gap function.

In conclusion, we discuss the Andreev reflection and the Josephson effect in the $\alpha - T_3$ lattice-based superconducting junction by solving the BdG equation. In the regime of SAR, the probability of Andreev reflection decreases as the parameter α increases when the incident energy of the electron is small. As the incident energy increases, the probability of Andreev reflection increases as the parameter α increases. There is an interesting property that the Andreev reflection with approximate all-angle perfect transmission happens in the case of $\alpha = 1$ when the incident energy approaches the superconducting energy gap function.

In the regime of ARR, the probability of Andreev reflection increases as α increases regardless of the incident energy of electron. Interestingly, when the incident energy approaches the superconducting energy gap function, the Andreev reflection with approximate all-angle perfect transmission happens regardless of the value of α , which is different from the case in the regime of SAR.

The measurable differential conductances of the NS junction in experiments are shown in these two regimes. We find that the differential conductances show the same property that their values increase as α increases generally in both regimes. Additionally, there is a difference that the value of differential conductance tends to $2G_0$ regardless of the value of α when the incident energy ε approaches the superconducting energy gap function Δ_0 in the case of $E_F \gg \varepsilon$.

In addition, we find that the $\alpha - T_3$ lattice-based Josephson current increases as α increases. The critical Josephson cur-

rents oscillate as the length of the junction varies and approach the same value when the length of the junction approaches zero in the different values of α . This paper gives the properties of continuous evolution of the Andreev reflection and the Josephson effect when the pseudospin of the fermion varies from pseudospin $S = \frac{1}{2}$ to pseudospin $S = 1$ continuously.

ACKNOWLEDGMENTS

This paper was supported by the National Natural Science Foundation of China (Grant No. 11747019, No. 11804167, No. 11804291, and No. 61874057), the Natural Science Foundation of Jiangsu Province (Grant No. BK20180890 and No. BK20180739), the Innovation Research Project of Jiangsu Province (Grant No. CZ0070619002), and NJUPT-SF (Grant No. NY218128).

-
- [1] K. S. Novoselov, A. K. Geim, S. V. Morozov, D. Jiang, Y. Zhang, S. V. Dubonos, I. V. Grigorieva, and A. A. Firsov, *Science* **306**, 666 (2004).
- [2] C.-C. Liu, W. Feng, and Y. Yao, *Phys. Rev. Lett.* **107**, 076802 (2011).
- [3] K. S. Novoselov, D. Jiang, F. Schedin, T. J. Booth, V. V. Khotkevich, S. V. Morozov, and A. K. Geim, *Proc. Natl. Acad. Sci. USA* **102**, 10451 (2005).
- [4] L. Li, Y. Yu, G. J. Ye, Q. Ge, X. Ou, H. Wu, D. Feng, X. H. Chen, and Y. Zhang, *Nat. Nanotechnol.* **9**, 372 (2014).
- [5] A. Molle, J. Goldberger, M. Houssa, Y. Xu, S.-C. Zhang, and D. Akinwande, *Nat. Mater.* **16**, 163 (2017).
- [6] D. Bercioux, D. F. Urban, H. Grabert, and W. Häusler, *Phys. Rev. A* **80**, 063603 (2009).
- [7] B. Dóra, J. Kailasvuori, and R. Moessner, *Phys. Rev. B* **84**, 195422 (2011).
- [8] Z. Lan, N. Goldman, A. Bermudez, W. Lu, and P. Ohberg, *Phys. Rev. B* **84**, 165115 (2011).
- [9] J. D. Malcolm and E. J. Nicol, *Phys. Rev. B* **90**, 035405 (2014).
- [10] A. Raoux, M. Morigi, J.-N. Fuchs, F. Piéchon, and G. Montambaux, *Phys. Rev. Lett.* **112**, 026402 (2014).
- [11] F. Piéchon, J.-N. Fuchs, A. Raoux, and G. Montambaux, *J. Phys.: Conf. Ser.* **603**, 012001 (2015).
- [12] J. D. Malcolm and E. J. Nicol, *Phys. Rev. B* **92**, 035118 (2015).
- [13] E. Illes, J. P. Carbotte, and E. J. Nicol, *Phys. Rev. B* **92**, 245410 (2015).
- [14] S. K. Firoz Islam and P. Dutta, *Phys. Rev. B* **96**, 045418 (2017).
- [15] B. Dey and T. K. Ghosh, *Phys. Rev. B* **98**, 075422 (2018).
- [16] C.-Z. Wang, C.-D. Han, H.-Y. Xu, and Y.-C. Lai, *Phys. Rev. B* **99**, 144302 (2019).
- [17] T. Louvet, P. Delplace, A. A. Fedorenko, and D. Carpentier, *Phys. Rev. B* **92**, 155116 (2015).
- [18] J. Wang, J. F. Liu, and C. S. Ting, *Phys. Rev. B* **101**, 205420 (2020).
- [19] R. Shen, L. B. Shao, B. Wang, and D. Y. Xing, *Phys. Rev. B* **81**, 041410(R) (2010).
- [20] D. F. Urban, D. Bercioux, M. Wimmer, and W. Häusler, *Phys. Rev. B* **84**, 115136 (2011).
- [21] E. Illes and E. J. Nicol, *Phys. Rev. B* **95**, 235432 (2017).
- [22] Y. Betancur-Ocampo, G. Cordourier-Maruri, V. Gupta, and R. de Coss, *Phys. Rev. B* **96**, 024304 (2017).
- [23] E. Illes and E. J. Nicol, *Phys. Rev. B* **94**, 125435 (2016).
- [24] T. Biswas and T. K. Ghosh, *J. Phys.: Condens. Matter* **28**, 495302 (2016).
- [25] T. Biswas and T. K. Ghosh, *J. Phys.: Condens. Matter* **30**, 075301 (2018).
- [26] E. V. Gorbar, V. P. Gusynin, and D. O. Oriekhov, *Phys. Rev. B* **99**, 155124 (2019).
- [27] E. V. Gorbar, V. P. Gusynin, and D. O. Oriekhov, *Phys. Rev. B* **103**, 155155 (2021).
- [28] L. Chen, J. Zuber, Z. Ma, and C. Zhang, *Phys. Rev. B* **100**, 035440 (2019).
- [29] M.-W. Alam, B. Souayah, and S. K. Firoz Islam, *J. Phys.: Condens. Matter* **31**, 485303 (2019).
- [30] D. Bercioux, N. Goldman, and D. F. Urban, *Phys. Rev. A* **83**, 023609 (2011).
- [31] B. Dey and T. K. Ghosh, *Phys. Rev. B* **99**, 205429 (2019).
- [32] B. Dey, P. Kapri, O. Pal, and T. K. Ghosh, *Phys. Rev. B* **101**, 235406 (2020).
- [33] S. Cheng, H. Yin, Z. Lu, C. He, P. Wang, and G. Xianlong, *Phys. Rev. A* **101**, 043620 (2020).
- [34] J. Wang and J.-F. Liu, *Phys. Rev. B* **103**, 075419 (2021).
- [35] A. Iurov, G. Gumbs, and D. Huang, *Phys. Rev. B* **99**, 205135 (2019).
- [36] A. Iurov, L. Zhemchuzhna, D. Dahal, G. Gumbs, and D. Huang, *Phys. Rev. B* **101**, 035129 (2020).
- [37] M. Vigh, L. Oroszlány, S. Vajna, P. San-Jose, G. Dávid, J. Cserti, and B. Dóra, *Phys. Rev. B* **88**, 161413(R) (2013).
- [38] E. Tang, J.-W. Mei, and X.-G. Wen, *Phys. Rev. Lett.* **106**, 236802 (2011).
- [39] K. Sun, Z. Gu, H. Katsura, and S. Das Sarma, *Phys. Rev. Lett.* **106**, 236803 (2011).
- [40] T. Neupert, L. Santos, C. Chamon, and C. Mudry, *Phys. Rev. Lett.* **106**, 236804 (2011).
- [41] Z. Liu, Z.-F. Wang, J.-W. Mei, Y.-S. Wu, and F. Liu, *Phys. Rev. Lett.* **110**, 106804 (2013).

- [42] M. G. Yamada, T. Soejima, N. Tsuji, D. Hirai, M. Dincă, and H. Aoki, *Phys. Rev. B* **94**, 081102(R) (2016).
- [43] N. Su, W. Jiang, Z. Wang, and F. Liu, *Appl. Phys. Lett.* **112**, 033301 (2018).
- [44] K. Cai, M. Yang, H. Ju, S. Wang, Y. Ji, B. Li, K. W. Edmonds, Y. Sheng, B. Zhang, N. Zhang, S. Liu, H. Zheng, and K. Wang, *Nat. Mater.* **16**, 712 (2017).
- [45] Y. Cao, Y. Sheng, K. W. Edmonds, Y. Ji, H. Zheng, and K. Wang, *Adv. Mater.* **32**, 1907929 (2020).
- [46] A. F. Andreev, *Sov. Phys. JETP* **19**, 1228 (1964).
- [47] C. W. J. Beenakker, *Phys. Rev. Lett.* **97**, 067007 (2006).
- [48] J. Linder and T. Yokoyama, *Phys. Rev. B* **89**, 020504(R) (2014).
- [49] L. Majidi, H. Rostami, and R. Asgari, *Phys. Rev. B* **89**, 045413 (2014).
- [50] J. Linder and T. Yokoyama, *Phys. Rev. B* **95**, 144515 (2017).
- [51] X. Zhou, *Phys. Rev. B* **102**, 045132 (2020).
- [52] B. D. Josephson, *Phys. Lett.* **1**, 251 (1962).
- [53] B. D. Josephson, *Rev. Mod. Phys.* **46**, 251 (1974).
- [54] P. W. Anderson and J. M. Rowell, *Phys. Rev. Lett.* **10**, 230 (1963).
- [55] I. O. Kulik, *Sov. Phys. JETP* **30**, 944 (1970).
- [56] A. I. Buzdin, L. N. Bulaevskii, and S. V. Panyukov, *Pis'ma Zh. Eksp. Teor. Fiz.* **35**, 147 (1982) [*JETP Lett.* **35**, 178 (1982)].
- [57] A. I. Buzdin, *Rev. Mod. Phys.* **77**, 935 (2005).
- [58] V. V. Ryazanov, V. A. Oboznov, A. Yu. Rusanov, A. V. Veretennikov, A. A. Golubov, and J. Aarts, *Phys. Rev. Lett.* **86**, 2427 (2001).
- [59] T. Yamashita, K. Tanikawa, S. Takahashi, and S. Maekawa, *Phys. Rev. Lett.* **95**, 097001 (2005).
- [60] A. Buzdin, *Phys. Rev. Lett.* **101**, 107005 (2008).
- [61] H. Sickinger, A. Lipman, M. Weides, R. G. Mints, H. Kohlstedt, D. Koelle, R. Kleiner, and E. Goldobin, *Phys. Rev. Lett.* **109**, 107002 (2012).
- [62] T. Yokoyama, M. Eto, and Y. V. Nazarov, *Phys. Rev. B* **89**, 195407 (2014).
- [63] K. N. Nesterov, M. Houzet, and J. S. Meyer, *Phys. Rev. B* **93**, 174502 (2016).
- [64] F. Dolcini, M. Houzet, and J. S. Meyer, *Phys. Rev. B* **92**, 035428 (2015).
- [65] M. Alidoust and H. Hamzeshpour, *Phys. Rev. B* **96**, 165422 (2017).
- [66] X. Zhou and G. Jin, *Phys. Rev. B* **95**, 195419 (2017).
- [67] X. Feng, Y. Liu, Z.-M. Yu, Z. Ma, L. K. Ang, Y. S. Ang, and S. A. Yang, *Phys. Rev. B* **101**, 235417 (2020).
- [68] M. Titov and C. W. J. Beenakker, *Phys. Rev. B* **74**, 041401(R) (2006).
- [69] P. G. de Gennes, *Superconductivity of Metals and Alloys* (Benjamin, New York, 1966).
- [70] G. E. Blonder, M. Tinkham, and T. M. Klapwijk, *Phys. Rev. B* **25**, 4515 (1982).
- [71] S. S. Wang, Y. Liu, Z.-M. Yu, X.-L. Sheng, L. Y. Zhu, S. Guan, and S. A. Yang, *Phys. Rev. Mater.* **2**, 104003 (2018).
- [72] C. Hua, S. Li, Z.-A. Xu, Y. Zheng, S. A. Yang, and Y. Lu, *Adv. Sci.* **7**, 1901939 (2020).
- [73] F. Wang and Y. Ran, *Phys. Rev. B* **84**, 241103(R) (2011).
- [74] J. Linder and A. Sudbø, *Phys. Rev. B* **77**, 064507 (2008).
- [75] J. Linder, A. M. Black-Schaffer, T. Yokoyama, S. Doniach, and A. Sudbø, *Phys. Rev. B* **80**, 094522 (2009).
- [76] H. Goudarzi and M. Khezerlou, *Physica E* **44**, 2082 (2012).
- [77] S. Ahmadvani and M. V. Hosseini, *J. Phys.: Condens. Matter* **32**, 315504 (2020).